Growth, structure, and electronic properties of nonpolar thin films on a polar substrate: Cr_{2}O_{3} on ZnO (0001) and ZnO (0001[over ¯])

X. Zhu, M. D. Morales-Acosta, J. Shen, F. J. Walker, J. J. Cha, and E. I. Altman

The Growth, Structure and Electronic Properties of Non-Polar Thin Films on a Polar Substrate: Cr$_2$O$_3$ on ZnO (0001) and ZnO (000$\overline{1}$)

X. Zhu[1,2], M.D. Morales-Acosta[1,3], J. Shen[1,4], F.J. Walker[1,3], J. J. Cha[1,4] and E.I. Altman[1,2,*]

[1]*Center for Research on Interface Structures and Phenomena (CRISP), Yale University, New Haven, CT 06520, USA*

[2]*Department of Chemical and Environmental Engineering, Yale University, New Haven, CT 06520, USA*

[3]*Department of Applied Physics, Yale University, New Haven, CT 06520, USA*

[4]*Department of Mechanical Engineering and Material Science, Yale University, New Haven, CT 06520, USA*

Abstract

The growth and geometric and electronic structures of Cr$_2$O$_3$ layers on the polar ZnO surfaces were characterized to determine how polar substrates can influence the properties of non-polar films. Photoelectron spectroscopy (XPS and UPS), high resolution transmission electron microscopy (HRTEM), electron diffraction (RHEED and LEED), and x-ray diffraction and reflectivity (XRD and XRR) were employed to characterize the growth mode, film quality and interfacial electronic properties. Chromium oxide growth on ZnO (000$\overline{1}$) and (0001) followed the same trends: two dimensional growth with initial disorder followed by the formation of epitaxial Cr$_2$O$_3$ (0001). Despite the initial disorder, HRTEM and XRD/XRR measurements on thicker films revealed an abrupt interface with the Cr$_2$O$_3$ lattice extending all the way to the interface. This indicates that above a critical thickness of 10 - 15 Cr-O$_3$-Cr repeat units the entire film reorganizes into an ordered structure. It is postulated that the oxygen remained ordered throughout the growth but that the chromium initially filled interstices randomly in the oxygen sublattice which allowed the film to eventually grow with a well-defined epitaxial relationship with the substrate. The polar interfaces showed a small band offset that decayed with increasing film thickness, suggesting that the compensating charges at the interface

may partially migrate to the film surface. No evidence of formal changes in the Cr oxidation state at the interfaces was seen. On the other hand, statistical analyses of UPS valence band spectra revealed an enhanced density of states near the valence band edge for Cr_2O_3 on ZnO (0001), consistent with stabilization of the positive interface by filling surface electronic states. In contrast, no significant valence band differences were observed between bulk Cr_2O_3 and thin Cr_2O_3 layers on ZnO ($000\bar{1}$) suggesting a different charge compensation mechanism on the negative surface. The potential impact of these findings on the surface properties of chromium oxide thin films is discussed.

PACS number(s): 68.35.-p, 68.47.Gh, 68.55.A-

I. Introduction

In polar materials, a net dipole can be associated with each repeat unit along a crystallographic axis. The propagation of the electric dipole, however, will cause the surface energy to diverge and so oppositely poled surfaces must be charge compensated in distinct ways. As a consequence, oppositely poled surfaces are expected to demonstrate different surface electronic, structural, and chemical properties.[1-3] Ferroelectric materials are an important subset of polar materials whose polarization direction can be switched by applying an external electric field. This effect allows one to envision materials with switchable surface properties.[1, 4-7] These features highlight polarization as a mechanism to tailor surface chemistry and catalytic properties that has largely not been exploited. Although it is not ferroelectric, the oppositely poled surfaces of ZnO display dramatically different reactivities.[8-15] Therefore, in this paper the interaction of non-polar Cr_2O_3 with the ZnO (0001) and (000$\bar{1}$) surfaces is explored with the goal of determining how much substrate polarization can impact the properties of a thin non-polar layer. It will be shown that despite initial disorder, Cr_2O_3 (0001) grows epitaxially on both ZnO substrates with an abrupt interface. The thinnest films display a band offset consistent with an interfacial dipole. In addition, new electronic states are observed at the interface with the positively poled ZnO surface that may alter the reactivity of the Cr oxide film.

The potential to induce unique, and possibly switchable, electronic, magnetic, and chemical properties at interfaces between polar and non-polar materials has motivated a great deal of research in recent years. Regarding electronic properties, a noteworthy example is the emergence of conductivity at the interface between the polar insulator $LaAlO_3$ (001) and the non-polar insulator $SrTiO_3$.[16-18] The conductivity can be readily explained by charge compensation of the positive interface by filling $SrTiO_3$ electronic states, although photoelectron spectroscopy

measurements have failed to detect any band offset indicative of the expected interface dipole.[19]

For chemical properties, the interest is due to the dearth of materials that exhibit both interesting polarization and catalytic properties. For example, the common ferroelectric materials $LiNbO_3$ and $PbTiO_3$ display polarization direction-dependent adsorption of polar molecules but the thermodynamically favored surfaces of both materials are catalytically inert.[20-23] Theoretical studies have suggested that ultrathin transition metal layers on ferroelectric surfaces can display unique catalytic properties. For example, it has been suggested that CO can dissociate on Pt on negatively poled $PbTiO_3$,[24] chemistry that is not observed on any known form of Pt. While early experiments suggested that ferroelectric polarization can influence CO oxidation rates on transition metals,[25] more recent experiments revealed no effect of the substrate polarization on the interaction of CO with transition metals.[26] The lack of any effect could be attributed to the difficulty in forming the atomically dispersed films required to affect the properties of a metal.[26] Therefore, we turn our attention to polar interfaces of catalytically interesting non-polar oxides that may be grown epitaxially, layer-by-layer.

Chromium (III) oxide based catalysts have been well-studied for a number of reactions including ethylene polymerization,[27] alkane dehydrogenation,[28-30] and the synthesis, isomerization and disproportionation of chloro-fluorocarbons.[31, 32] Chromia crystallizes in the corundum structure built up by stacking non-polar $Cr-O_3-Cr$ tri-layers along the [0001] direction as pictured in Fig. 1a; for the remainder of this paper a Cr_2O_3 repeat unit (RU) is defined as a single $Cr-O_3-Cr$ tri-layer and will be used as the unit for Cr_2O_3 coverage. The (0001) surface exposes a hexagonal O plane with 1/3 of the octahedral sites filled by Cr; see Fig. 1b. Meanwhile, wurtzite-structured ZnO is a polar crystal constructed by stacking alternating hexagonal O and Zn layers along [0001] as illustrated in Fig. 1c. The bulk-terminated (0001)

surface exposes a hexagonal Zn plane; see Fig. 1d. There is a net dipole within the ZnO repeat unit along [0001] and the propagation of this dipole will diverge without charge compensation. It is commonly believed that the nominally oxygen-terminated $(000\bar{1})$ surface is typically compensated by protons even under UHV conditions, while the nominally Zn-terminated (0001) surface is compensated by negative charges at the edges of surface pits.[33-39] The positively poled surface is generally more reactive.[8-11] The hexagonal oxygen sublattices of Cr_2O_3 and ZnO are structurally similar, although the O atoms are much more closely packed in Cr_2O_3 than in ZnO, 0.285 nm apart versus 0.325 nm apart in ZnO. Despite the large lattice mismatch, it has been shown that high-quality epitaxial ZnO can be grown on Cr_2O_3 (0001) with the expected 30° rotation.[40, 41]

The growth of Cr_2O_3 on positively and negatively poled ZnO (0001) was characterized using low energy and reflection high energy electron diffraction (RHEED and LEED), high resolution transmission electron microscopy (HRTEM) and x-ray diffraction/reflectivity (XRD/XRR) measurements, while the electronic structure of the interface and film were characterized using x-ray and ultraviolet photoelectron spectroscopies (XPS and UPS). For both ZnO surfaces it will be shown that Cr_2O_3 growth is two dimensional (2D) and that although the initial growth is disordered, the Cr_2O_3 films are ultimately epitaxial all the way to the interface. A small band offset is seen between films on oppositely poled surfaces that decays with increasing film thickness suggesting that at least some of the compensating charges migrate to the film surface. There was no evidence of changes in the Cr oxidation state at any point indicating that charge compensation does not involve formal oxidation/reduction of the Cr cations. On the other hand, UPS spectra revealed enhanced emission near the valence band edge of thin Cr_2O_3 thin films on positively poled ZnO consistent with charge compensation involving

5

filling of interfacial electronic states; no changes in the valence band were observed on the negatively poled ZnO. The impact of the results on the chemical properties of thin non-polar films on polar substrates will be discussed.

II. Experimental

Growth, electron diffraction, and photoelectron spectroscopy experiments were performed using an interconnected three-chamber ultra-high vacuum (UHV) system consisting of a growth chamber, an analysis chamber, and a microscopy chamber, which has been described in detail previously.[42] The turbo-pumped growth chamber is equipped with effusion cells and electron beam evaporators; Cr was deposited using one of the electron beam evaporators. Chromium pieces (99.997% purity) for deposition were obtained from Alfa Aesar. The flux from each source could be monitored and controlled using independent quartz crystal oscillators (QCOs) near the source positions. The tooling factors for the QCOs were measured by moving an additional QCO to the sample position. The QCO was additionally calibrated by comparing the thickness of a film determined by measuring the spacing of the thickness fringes in XRR measurements with the thickness expected based on QCO readings assuming Cr metal was deposited onto the sensor. A differentially pumped 20 keV electron gun and a fluorescent screen mounted on the opposite side of the chamber were used to obtain RHEED patterns during growth. The growth chamber was also equipped with a microwave electron cyclotron resonance plasma source pointed at the growth position that could be used to generate reactive oxygen species. The ion-pumped analysis chamber was equipped with a double pass cylindrical mirror analyzer (DP-CMA), a dual anode x-ray source for XPS, a He discharge lamp for ultraviolet photoelectron spectroscopy (UPS) and rear-view LEED optics. The typical base pressures were 1×10^{-9} Torr in the growth chamber and 1×10^{-10} Torr in the analysis chamber. Samples were

mounted on transferable sample holders with a chromel-alumel thermocouple mounted to the baseplate behind the sample and were heated by a combination of radiation and electron beam heating by a filament behind the sample baseplate. Previous results indicate that placing the thermocouple on the backing plate does not lead to substantial errors in the temperature measurement.[43]

The substrates were 5 x 5 mm by 0.5 mm thick ZnO (0001) and ZnO (000$\bar{1}$) plates obtained from MTI corporation. The substrates were polished on one side and oriented within ±0.5° of [0001]. Prior to insertion into the UHV system, the ZnO samples were annealed in flowing air at 1200 K for 10-15 hours.[44] Upon insertion into the UHV chamber, both ZnO (0001) and ZnO (000$\bar{1}$) samples were cleaned in the effluent of the oxygen plasma source at 575K for an hour to remove impurities, mainly carbon. Then the samples were sputtered with 500 eV Ar ions for 15 minutes and annealed in UHV at 575K for three cycles. Sharp hexagonal (1x1) LEED patterns were observed after this process. Prior work has shown that these conditions yield negative surfaces passivated by H and positive surfaces by pits with negative charges at their edges.[33, 36] Removal of the surface H from the (000$\bar{1}$) surface leads to (2x2) and (5x5) reconstructions[45] which were not seen here and so it is assumed that the starting negative surface for Cr oxide growth was terminated by H.

Chromium oxide films were grown between 845 – 900 K in O_2 background pressures ranging from 6x10^{-5} to 1x10^{-7} Torr. Core-level XPS spectra were excited with non-monochromatic 1253.6 eV Mg K$_{\alpha1,\alpha2}$ radiation; spectra were taken with 0.8 eV overall system resolution. The XPS spectra were corrected for x-ray satellite lines at 1245.1 eV and 1243.5 eV. The axis of the DPCMA was normal to the sample surface during all photoemission experiments. Because charging of the semiconducting zinc oxide tended to shift the kinetic energy of the XPS

peaks, the binding energies were referenced by positioning the Zn $2p_{3/2}$ peaks at a binding energy of 1022.0 eV;[46] the corrections for charging were no more than 1 eV. For thick Cr oxide films where the Zn was no longer visible, the O 1s peak was used as a reference. In this case, the position of the O 1s peak was set at the binding energy seen for 8-10 RU thick Cr oxide films (corrected for any shifts in the Zn peaks) where the Zn 2p peaks were still visible but small compared to the Cr 2p peaks, and thus the O 1s peak was dominated by the Cr_2O_3 contribution. The XPS peak locations were obtained by fitting the data to mixed Gaussian-Lorentzian peak shapes following subtraction of a Shirley background. Uncertainties in the peak positions were estimated using a Monte Carlo approach implemented in CasaXPS. [47-49]

The UPS spectra were obtained using He II (40.8 eV) radiation; spectra were collected with the DPCMA resolution set to 0.24 eV. The UPS spectra were corrected for satellite lines at 48.37 eV in the discharge lamp output.

RHEED patterns were collected at room temperature both prior to and after the growth as well as at the growth temperature during growth. All LEED patterns were collected at room temperature. The bulk phase and crystallographic orientation of the films were characterized ex situ using HRTEM, XRD and XRR. The TEM data was acquired with a FEI Tecnai Osiris 200 kV. XRD and XRR measurements were performed with a Rigaku SmartLab x-ray diffractometer with a crystal Ge (220) monochromator on the incident beam and Cu K_α radiation, operated at 45 kV and 200 mA.

III. Results

A. Evolution of Cr_2O_3 Film Structure

During each growth, RHEED, LEED, XPS, and UPS data were collected to determine the morphology and chemical nature of the film. Fig. 2a shows how the RHEED pattern along the

substrate [1$\bar{1}$00] direction changed as chromium oxide was deposited onto ZnO (0001) at 845 K in 1.0×10^{-7} Torr O_2. By 4 RU the bright spots indicative of a flat substrate gave way to a very faint pattern with the same periodicity. A new pattern appeared by 11 RU with a periodicity close to three times that of the original pattern. This pattern did not change further as the thickness was increased to 70 RU. A rough tripling of the periodicity along the substrate [1$\bar{1}$00] direction is consistent with a transition from a cation sublattice identical to that of the oxygen sublattice, as in ZnO, to a corundum structure in which the Cr cations fill one third of the octahedral sites in the oxygen sublattice in a $\left(\sqrt{3} \times \sqrt{3} \right) R30^0$ pattern. The streaks indicate a relatively flat surface with a distribution of terrace widths extending below the roughly 20 nm transfer width of the RHEED measurement. The same RHEED transition was also seen along the (2$\bar{1}\bar{1}$0) direction rotated 60^o from the (1$\bar{1}$00) direction which demonstrates that the film is hexagonal. As shown in Fig. 2b, results for ZnO (000$\bar{1}$) were qualitatively similar: the substrate RHEED pattern gradually decayed and was replaced by a pattern with roughly three times the periodicity. For the negatively poled surface, however, the substrate pattern completely vanished at 5 RU and it took longer for the new $\approx 3\times$ pattern to emerge. Once the $\approx 3\times$ pattern appeared it did not change up to 80 RU.

A more complete picture of the reciprocal surface lattice was obtained through LEED measurements. As illustrated in Figs. 3 and 4, the results reinforce the conclusions made from the RHEED data. On both ZnO surfaces, the substrate pattern initially weakened, or disappeared entirely for the negatively poled surface, before a new pattern appeared between 10 – 15 RU that persisted thereafter. The new pattern is rotated 30° with respect to the original one with the spots roughly $\sqrt{3}/_{3}$ closer to the center. Note that after depositing Cr oxide, the spots near the original (1, 0) spots are closer to the edge of the screen, consistent with the expected decreased spacing of

the oxygen sublattice in going from ZnO to Cr_2O_3. Thus, the electron diffraction results all point to the eventual formation of epitaxial Cr_2O_3 (0001) rotated 30^0 in plane with respect to the ZnO substrate.

The growth mode was characterized by analyzing the decay of the Zn 2p and the growth of the Cr 2p core level XPS peaks as a function of coverage. For these experiments, the Cr 2p, Zn 2p and O 1s spectra were recorded after chromium oxide was incrementally added to the surface. The ratios of the Cr $2p_{3/2}$ and Zn $2p_{3/2}$ peak areas to the O 1s peak areas were normalized to peak ratios for a thick Cr_2O_3 film for Cr and for the bare substrate for Zn. Fig. 5 shows a comparison between the experimentally measured Cr $2p_{3/2}$ and Zn $2p_{3/2}$ to O 1s peak integral ratios and those calculated assuming layer-by-layer growth, considering the Beer-Lambert Law with electron mean free paths obtained from the universal curve for mean free paths (0.8 nm for Zn and 1.21 nm for Cr and O),[50] and taking into account the 1.495 times higher O atom density in Cr_2O_3 versus ZnO. For both the positively and negatively poled surfaces the Zn peak decays and the Cr peak grows at least as rapidly as anticipated based on the above assumptions; therefore, it is concluded that the growth is 2D. For 2D growth, it is curious how all evidence of order can be lost for the first couple of nanometers yet ultimately crystalline films with a well-defined epitaxial relationship with the substrate can still form. It will be shown in the following Section that once order was observed at the surface, the entire film was ordered, thereby providing a connection between the crystallographic orientation of the substrate and the growing film.

To determine if order could be induced throughout the growth process, Cr oxide growth at higher substrate temperatures was attempted. At 905 K and 5.0×10^{-6} Torr O_2 pressure, the initial diminution of the diffraction patterns was still observed. At the higher temperature,

however, a roughly (2×2) LEED pattern emerged by 6 RU. Core level XPS spectra revealed a much higher Zn intensity than growth at lower temperatures. The near doubling of the periodicity is consistent with the formation of [111]-oriented, spinel-structured $ZnCr_2O_4$ with a lattice spacing of 0.588 nm.[51, 52] Therefore, the growth temperature is limited by the onset of Cr/Zn interdiffusion and the resulting formation of zinc chromate.

B. Bulk and Interfacial Structural Characterization

X-ray diffraction was used to characterize the bulk structure of the chromium oxide films grown at 845 K while XRR was used to characterize the surface and interfacial roughness. As shown in Fig. 6a, the XRD θ-2θ scans obtained after depositing thick Cr_2O_3 films onto ZnO (0001) and (000$\bar{1}$) both showed peaks near 40° and 86°, consistent with the (0 0 6) and (0 0 12) Cr_2O_3 reflections. The measured out-of-plane spacing was 1.3506 nm for Cr_2O_3 on ZnO(0001) and 1.3568 nm for Cr_2O_3 on ZnO(000$\bar{1}$), which closely correspond to the 1.3597 nm expected along the bulk Cr_2O_3 [0 0 1] direction,[53] indicating that the films exposed the Cr_2O_3 basal plane. The out-of-plane spacing for both films is slightly smaller than literature values for bulk Cr_2O_3 which can be a result of in-plane tension at the interface due to lattice mismatch.[53] No peaks due to other Cr oxides could be detected, reinforcing the conclusion that growth at 845 K produces only c-axis oriented Cr_2O_3.

From the XRR θ-2θ scans in Fig. 6b, the surface and interfacial roughnesses in addition to the thickness of the Cr_2O_3 films grown on ZnO (0001) and ZnO (000$\bar{1}$) at 845 K could be determined. The results indicate that the film on the (0001) substrate was 15.6 nm (≈70 RU) thick and that on the (000$\bar{1}$) substrate 17.1 nm (≈75 RU) thick. The decay rates of the oscillations indicate that the interfaces are smooth with roughnesses near the detection limit of the measurement, less than 20 pm. The surface roughnesses obtained from the overall decay rate

of the signals are also small, less than 30 pm for both surfaces. These data indicate that no measurable Zn-Cr interdiffusion occurs, consistent with the XPS data in Fig. 5. Also, despite the lack of any surface diffraction patterns during the initial growth, there is little evidence of interfacial roughness.

To help understand how films that initially grow disordered eventually develop order and atomically-smooth abrupt interfaces, the film structure was also characterized using cross-sectional HRTEM imaging in conjunction with Energy-dispersive X-ray spectral (EDX) mapping with the electron beam in the scanning mode; results are shown in Fig. 7 for Cr_2O_3/ZnO (0001). Consistent with the XRR and XPS data, the EDX maps in Fig. 7b reveal an atomically abrupt transition from the ZnO substrate to the Cr oxide film, as well as the increase in O atom density expected in going from ZnO to Cr_2O_3. The HRTEM image in Fig. 7a that shows the same region reveals lattice fringes with the expected spacing for Cr_2O_3 extending all the way to the interface, indicating that once order is established after depositing $10 - 15$ RU Cr_2O_3, the entire film orders. This explains how the well-defined epitaxial relationship takes hold despite the initial disorder and how the abrupt interface forms. The image also reveals a number of dislocations near the interface which is not surprising given the large lattice mismatch.

C. Electronic Properties of the Cr_2O_3/ZnO Interfaces

Comparison of the Cr core level XPS peaks for Cr_2O_3 on oppositely poled ZnO surfaces can be viewed as a sensitive probe of the charge compensation mechanism of the polar system. Figure 8 shows the evolution of the Cr 2p and Zn 2p core level spectra as Cr oxide was incrementally added to the ZnO surfaces. As mentioned in the Experimental section, the Zn $2p_{3/2}$ peaks were set as a reference at 1022.0 eV, and so the Zn peaks cannot shift. More significantly, on both ZnO surfaces the Zn peaks simply fade away without any evidence of new peaks

12

emerging or broadening that could be due to either interfacial reactions or oxidation/reduction of interfacial Zn playing a role in charge compensation. Meanwhile, Fig. 8b shows that on ZnO (0001), the binding energies of the Cr $2p_{1/2}$ and $2p_{3/2}$ peaks were 587.1 eV ± 0.3 eV and 577.1 eV ± 0.3 eV regardless of the coverage. These values are slightly higher than those usually reported for Cr_2O_3, typically 567.8 eV for the $2p_{3/2}$ peak.[54-56] For CrO_3, however, the Cr $2p_{3/2}$ peak position is 1.5 eV higher at 578.3 eV.[56] Meanwhile the XPS peaks for Cr^{4+} are unique in that they appear at lower binding energies than those of Cr^{3+} despite the higher oxidation state; reported Cr $2p_{3/2}$ peak positions for CrO_2 range from 576.3–576.4 eV.[55, 56] Divalent Cr^{2+} is relatively unstable with respect to oxidation to Cr^{3+} and is thus not expected to form under the growth conditions used here. Lastly, XPS peaks for Cr metal are at significantly lower binding energies than those for oxidized Cr.[57] Thus, despite the small mismatch between the observed and expected Cr $2p_{3/2}$ binding energy for Cr_2O_3 it is concluded that Cr is in the +3 oxidation state. On the other hand, Fig. 8d shows that as Cr oxide was added to ZnO ($000\bar{1}$), the Cr $2p_{1/2}$ and $2p_{3/2}$ peaks shifted by nearly 0.5 eV to lower binding energies. The Cr peaks also appeared at consistently higher binding energies on the negative surface. This is shown more clearly in Fig. 9 which compares the Cr $2p_{3/2}$ peak positions on the oppositely poled surface. As illustrated in Fig. 9, the binding energy difference between the Cr 2p peaks on the two ZnO surfaces is ≈0.5 eV at the lowest coverages, consistent with prior work by Piper et al. which revealed shifts of similar magnitude due to hydroxylation of the negative surface.[58] The energy difference then decayed but remained distinct over the range where both the Cr 2p and Zn 2p peaks were detectable. For all of these films the O 1s region was also analyzed. In accord with prior work that showed very similar O 1s binding energies for ZnO and Cr_2O_3,[59, 60] no significant changes in the O 1s peaks were seen with coverage or substrate polarization other than a slightly higher

binding energy on the negative surface at coverages where the Cr peaks were large compared to the Zn peaks.

Although the negatively poled surface could be compensated by positive charges generated by Cr oxidation at the interface to Cr^{4+} and the positive surface by Cr reduction to Cr^{2+} at the interface, the changes with coverage and the differences in the Cr 2p core level positions on the oppositely poled ZnO surfaces cannot be explained by oxidation/reduction of interfacial Cr. Both oxidation to Cr^{4+} and reduction to Cr^{2+} yield binding energies substantially lower than Cr^{3+}.[56, 61] Therefore, Cr oxidation/reduction at the interface would be expected to induce lower binding energy Cr 2p peaks on both ZnO surfaces at the lowest coverage that would decay as a higher binding energy peak due to Cr^{3+} increased in intensity as the Cr oxide thickened. Instead, spectra of the negative surface revealed a single peak that shifted to lower binding energies as the coverage was increased, while spectra for the positive surface showed no significant changes with coverage.

The consistently higher Cr 2p binding energy on the ZnO $(000\bar{1})$ surface can be explained by band offsets due to interfacial dipoles that occur at polar interfaces regardless of the charge compensation mechanism. For negatively poled ZnO which requires positive compensating charges, the dipole points away from the ZnO causing photoelectrons emitted above the dipolar layer to shift to apparently higher binding energies.[62] Meanwhile, the dipole points towards the substrate for the positively poled surface causing photoelectrons emitted above the dipolar layer to shift to apparently lower binding energies. Thus, even without any differences in chemical state, the Cr core levels would be expected to occur at higher binding energies on the negative surface, as observed. A dipolar layer restricted to the interface, however, should lead to a rigid shift of the Cr oxide XPS peaks on oppositely poled ZnO substrates

independent of coverage. The decreasing Cr 2p binding energies on the negatively poled ZnO substrate as the Cr_2O_3 film thickened suggests at least partial migration of the dipolar layer away from the interface. It should be noted that the observed Cr 2p binding energy shift with coverage occurred well before the disorder-order transition, eliminating Cr_2O_3 crystallization as the cause of the thickness-dependent shift.

Valence band spectra were analyzed with UPS to characterize the bonding at the interfaces. Series of spectra for Cr_2O_3 grown on the oppositely poled surfaces are shown in Fig. 10. In both cases the spectra were from single experimental runs in which the growths were interrupted to characterize the film properties before adding more Cr oxide. Starting with the bare substrates, although the oppositely poled surfaces are qualitatively similar with sharp peaks just below 10 eV that can be attributed to Zn 3d-derived bands and broader features between 3 – 8 eV that have been assigned to predominantly O 2p-derived bands, the spectra are not identical. The different intensities of the features in the O 2p-derived bands has been seen previously and assigned to the different structures of the (0001) and (000$\bar{1}$) surfaces.[63, 64] Not surprisingly, the spectra for the thick Cr_2O_3 films on both substrates are very similar to each other and to previously reported valence band spectra of bulk Cr_2O_3.[65] The distinct peak nearest the Fermi level has been assigned to emission from Cr 3d-derived states while the three peaks between 4 – 9 eV are attributed to bands derived from a mixture of O 2p and Cr 3d states.[66] Note that even after depositing 10 RU Cr_2O_3, which is sufficient to completely obstruct the Zn 3d peak, the UPS spectra for both substrates have not fully evolved into spectra characteristic of bulk Cr_2O_3. This result is not surprising given that the electron diffraction data indicate that the bulk Cr_2O_3 structure has not fully developed by this point.

The overlap of the ZnO and Cr_2O_3 spectral features in the valence band makes it difficult to isolate interfacial effects just by visually inspecting the spectra. To surmount this difficulty, the spectra for thin Cr_2O_3 films were fit as linear combinations of the spectra for the bare ZnO substrates and thick Cr_2O_3 films through spline interpolation and a general least squares method as illustrated in Fig. 11. The adjustable parameters were the intensities of the reference spectra, their lateral position, and a vertical offset. If there is no interfacial bonding and the thin Cr_2O_3 films are bulk-like then the fit would be perfect, suggesting that any residual would be due to either interfacial bonding or differences between thin and bulk Cr_2O_3. As illustrated in Fig. 11 for 1 RU Cr_2O_3 on the positive substrate, the peak at the valence band edge associated with filled Cr 3d states is significantly more intense than would be expected by just a linear combination of bulk ZnO and Cr_2O_3 spectra. Meanwhile, there is extra intensity just above 4 eV that could not be accounted for by a linear combination of the bulk spectra; the Zn 3d peak at 10 eV is unchanged. The result is two peaks in the residual curve centered just below 3 eV and near 4.6 eV. Fig. 12a shows the residual curves for the positive surface for Cr_2O_3 coverages between 0.5 and 10 RU. These curves reveal that the features just below 3 eV and near 4.6 eV increase in intensity up to 2 RU before their intensity falls some at 5 RU before declining substantially at 10 RU. Also note that at 2 and 5 RU, the linear combination of bulk spectra does not accurately predict the intensity of the Zn 3d peak. The persistence of the two peaks beyond 1 RU indicate that these electronic perturbations are not confined to the interface.

As detailed above, the bulk Cr_2O_3 geometric and electronic structures have not developed by 10 RU, suggesting that the failure to model the valence band of thin Cr_2O_3 layers on ZnO (0001) as a linear combination of bulk ZnO and Cr_2O_3 valence bands may be related to differences in the atomic arrangement of bulk and thin film Cr_2O_3. To test this hypothesis, the

16

UPS spectra for the thin films were also fit as linear combinations of bare ZnO (0001) and 10 RU thick Cr_2O_3 thin films. As shown in Fig. 12b, the resulting residual curves are similar to those in Fig. 12a suggesting that the observed features are a result of the interaction of the Cr_2O_3 film with the positive surface and not the structural disorder of the thin layers. Results for the negative surface reinforce this conclusion. As illustrated in Fig. 12c, the residual curves for the negative surface are flat below 6 eV except for a small dip between 3 – 4 eV for the 0.5 RU thick film. Because Cr_2O_3 growth on the positive and negative surfaces follow the same ordering transition above 10 RU, this result excludes differences between bulk and thin film Cr_2O_3 structures as the source of the distinct peaks in the residual curves on the positive surface. Finally, the features seen near 10 eV in the residual plots in Figs. 12c and 12d are due to a broadening of the Zn 3d peak following Cr oxide deposition onto the negative surface.

IV. Discussion

The growth of Cr_2O_3 on ZnO (0001) and (000$\bar{1}$) can be summarized as follows: (1) Zn-Cr intermixing limits the growth temperature to below 900 K; (2) the growth is 2D independent of the polarization direction; (3) also independent of the polarization direction the growth is initially disordered but by 15 RU epitaxial Cr_2O_3 forms; (4) once crystalline Cr_2O_3 forms it extends all the way to the interface resulting in an abrupt crystalline interface; (5) Cr 2p XPS binding energies are consistently higher on the negative surface; (6) the difference in Cr 2p binding energies on the opposite ZnO surfaces decays with coverage; (7) no evidence of formal changes in the Cr oxidation state are ever seen; and (8) UPS data reveal enhanced emission in spectral regions associated with the partially filled Cr 3d band and O 2p band for thin Cr_2O_3 on the positive surface.

It is remarkable that the Cr oxide films on both ZnO surfaces can become ordered with a well-defined epitaxial relationship with the substrate despite passing through a region where order is lost. The hexagonal oxygen sublattice shared by ZnO and Cr_2O_3 (0001) can provide a driving force to maintain a specific registry between the film and substrate, despite the large lattice mismatch and different preferred cation site symmetry. In this model, repulsion between oxygen anions across the Cr_2O_3/ZnO interface is minimized by continuing the substrate oxygen sublattice across the interface. The different O atom spacing and preferred cation sites for Cr (octahedral) and Zn (tetrahedral), as well as the lower cation density in Cr_2O_3; however, conspire to prevent the Cr from filling the sites it would in bulk Cr_2O_3. Rather, the Cr fills the interstices of the O sublattice in a highly disordered way. Evidence for a strained and defective ZnO oxygen sublattice filled with disordered Cr cations can be seen in the LEED pattern for the 4 RU thick Cr oxide film on the positive surface where a diffuse pattern with the same spacing as the substrate can still be seen even though the film is too thick to allow any substrate contribution. As the Cr oxide film thickens, the contribution of the disruption of the interface to the total energy of the film decreases until a critical thickness is reached where the energy gained by forming the bulk Cr_2O_3 structure offsets the cost of introducing dislocations near the interface that accommodate the lattice mismatch but no longer minimize ionic repulsions across the interface. The electron diffraction data indicate that this critical thickness is 10 – 15 RU. This model assumes that the Cr cations have sufficient mobility at the growth temperature to find their lowest energy sites, even after buried under 10 RU of oxide. The HRTEM results showing Cr_2O_3 lattice fringes extending all the way to the interface as well as the minimal interfacial roughness indicated by XRR measurements support this assumption.

Key questions regarding the growth of non-polar Cr_2O_3 on the polar ZnO surfaces concern the nature and location of the compensating charges. The photoelectron spectroscopy results provide insights into these issues. First, the higher binding energies of the Cr 2p core levels on the negative surface are consistent with the band offsets expected due to oppositely oriented dipolar layers compensating the polar/non-polar interfaces. The decay of the Cr 2p binding energy difference with increasing coverage suggests; however, that the dipolar layer can migrate to the surface as Cr oxide is added. For the negative surface where the Cr 2p binding energies decrease with coverage to approach those on the positive surface, adsorbed protons are considered to play an important role in charge compensation even under UHV conditions.[34-37] Thus, one can envision the protons continuously migrating to the surface as the Cr oxide film thickens. On the other hand, the positive ZnO surface is considered to be compensated by negative charges exposed at pit edges and so the question becomes what happens to these negative charges when the surface is covered by Cr_2O_3? The Cr 2p core level spectra for the positive surface remained in the region expected for Cr^{3+} and showed no evidence of reduced Cr^{2+} confined to the interface. Analysis of UPS spectra of the positive surface; however, show increased intensity from a valence band edge feature typically associated with the partially filled Cr 3d band suggesting at least partial charge transfer to Cr. These spectral features persist for at least 2 RU indicating that the charge transfer is not restricted to Cr directly at the interface. The failure of this charge transfer to produce significant shifts in the Cr core level positions could be due to the small amount of charge transfer as well as hybridization of the Cr 3d and O 2p levels which precludes attributing the intensity of the feature solely with charge transfer to Cr. Future work will focus on characterizing the oxidation state of Cr at the interface with Electron Energy-Loss Spectroscopy (EELS) during STEM measurements which can be more sensitive to small

changes in oxidation state than XPS. It should also be pointed out that the appearance of distinct valence band features for Cr oxide on the positive surface but not the negative surface is consistent with many experiments over the years that have shown that the positive surface can be highly reactive while the negative surface is largely inert.[8-11]

The results suggest that the Cr_2O_3 interface with ZnO (0001) is compensated at least in part by filling electronic states in the Cr_2O_3 film, while the interface with the negative ZnO (000$\bar{1}$) may be compensated by adsorption of positive charges, most likely in the form of protons. It is interesting to consider how these distinct mechanisms can alter the catalytic properties of Cr oxide. The catalytic activity of chromium oxide is often tied to the Lewis acidity or ability of surface Cr to accept electrons.[31, 32] For halocarbon reactions, increased Lewis acidity that accompanies halogen substitution, in particular fluorine, for oxygen is considered to increase the activity of the catalyst.[67-69] Replacing oxygen with more electronegative fluorine decreases the electron density around the Cr, thereby increasing its ability to accept electrons from adsorbed molecules. The UPS data suggest that supporting Cr_2O_3 on positively poled ZnO (0001) increases the electron density around surface Cr species implying a decreased Lewis acidity and thus modification of catalytic properties without a compositional change. The effect of charge compensating protons at the surface of Cr_2O_3/ZnO (000$\bar{1}$) on reactivity is more complex. Since the Cr electronic structure is not affected by the negative ZnO surface, the ability to bind molecules at exposed Cr surface sites should not be altered. The charge compensating proton, however, can alter the surface's activity for hydrogenation/dehydrogenation and oxidation reactions. Because the proton is required for charge compensation, it cannot be removed without replacing it with another positive charge; e.g. by also removing an oxygen anion to create a positively charged oxygen vacancy. Therefore, this strongly bound proton is not available for

20

reaction and can block oxygen surface sites that could otherwise abstract H from molecules adsorbed on the surfaces of bulk Cr_2O_3.[70] Finally, the results indicate that the effect of the ZnO substrate extends for at least two Cr_2O_3 layers and that the Cr_2O_3 grows layer-by-layer, thereby surmounting the problems encountered in trying to use polarization to manipulate the catalytic properties of transition metals.

V. Summary

The formation, structure, and electronic properties of the polar Cr_2O_3/ZnO $(000\bar{1})$ and Cr_2O_3/ZnO (0001) interfaces were characterized to understand how the polar substrate can influence the properties of the non-polar film. Chromium oxide growth was 2D independent of the substrate polarization direction. Also independent of the polarization direction, epitaxial Cr_2O_3 (0001) formed after initial disorder. The epitaxy was seen all the way to the interface indicating that Cr cations in the film are mobile at the 845 K growth temperature and that at a critical thickness between $10 - 15$ RU the driving force for forming bulk Cr_2O_3 exceeds the cost of introducing dislocations that accommodate the substantial lattice mismatch. The Cr 2p XPS binding energies were uniformly higher on the negative surface, consistent with oppositely oriented dipoles on the two ZnO surfaces creating a band offset. The difference between the Cr 2p binding energies on the two surfaces, however, was largest for very low Cr oxide coverages and then decayed, suggesting that some of the compensating charges migrate to the Cr oxide surfaces. At no point was there any indication of Cr oxidation states other than Cr^{3+} suggesting that charge compensation does not involve a formal change in the Cr oxidation state. On the other hand, analysis of valence band spectra revealed an excess occupation of a Cr 3d-derived peak at the valence band edge on ZnO (0001), consistent with charge compensation of the positive surface through filling of surface and interface electronic states. Meanwhile, this Cr 3d-

21

derived peak on ZnO ($000\bar{1}$) was indistinguishable from that on bulk Cr_2O_3 suggesting a different charge compensation mechanism on the negative surface. The ability to grow Cr_2O_3 2D on ZnO and the obvious differences in the Cr_2O_3 electronic structure on the opposite ZnO surfaces that extend for at least 2 RU make the Cr_2O_3/ZnO system attractive for studying the impact of substrate polarization on the surface properties of non-polar thin films.

Acknowledgements

References

[1] K. Garrity, A. M. Kolpak, S. Ismail-Beigi, and E. I. Altman, Advanced Materials **22**, 2969 (2010).

[2] J. Goniakowski, F. Finocchi, and C. Noguera, Reports on Progress in Physics **71**, 016501 (2008).

[3] N. Claudine, Journal of Physics: Condensed Matter **12**, R367 (2000).

[4] Z. Zhang, P. Sharma, C. N. Borca, P. A. Dowben, and A. Gruverman, Applied Physics Letters **97**, 243702 (2010).

[5] S. Habicht, R. J. Nemanich, and A. Gruverman, Nanotechnology **19**, 495303 (2008).

[6] M. H. Zhao, D. A. Bonnell, and J. M. Vohs, Surface Science **603**, 284 (2009).

[7] A. Kakekhani, and S. Ismail-Beigi, ACS Catalysis **5**, 4537 (2015).

[8] J. M. Vohs, and M. A. Barteau, Surface Science **176**, 91 (1986).

[9] B. Halevi, and J. M. Vohs, The Journal of Physical Chemistry B **109**, 23976 (2005).

[10] C. Kolczewski, M. Wühn, J. Albers, K. Weiss, V. Staemmler, and C. Wöll, The Journal of Chemical Physics **112**, 3909 (2000).

[11] S. Gil Girol, T. Strunskus, M. Muhler, and C. Wöll, The Journal of Physical Chemistry B **108**, 13736 (2004).

[12] J. Yang *et al.*, Journal of Alloys and Compounds **528**, 28 (2012).

[13] C. Kunze, M. Valtiner, R. Michels, K. Huber, and G. Grundmeier, Physical Chemistry Chemical Physics **13**, 12959 (2011).

[14] K. Kähler, M. C. Holz, M. Rohe, J. Strunk, and M. Muhler, ChemPhysChem **11**, 2521 (2010).

[15] C. Mateos-Pedrero *et al.*, Applied Catalysis B: Environmental **174**, 67 (2015).

[16] H. Chen, A. M. Kolpak, and S. Ismail-Beigi, Advanced Materials **22**, 2881 (2010).

[17] A. Ohtomo, and H. Y. Hwang, Nature **427**, 423 (2004).

[18] N. Reyren *et al.*, Science **317**, 1196 (2007).

[19] Y. Segal, J. H. Ngai, J. W. Reiner, F. J. Walker, and C. H. Ahn, Physical Review B **80**, 241107 (2009).

[20] Y. Yun, and E. I. Altman, Journal of the American Chemical Society **129**, 15684 (2007).

[21] Y. Yun, L. Kampschulte, M. Li, D. Liao, and E. I. Altman, The Journal of Physical Chemistry C **111**, 13951 (2007).

[22] D. Li *et al.*, Nature Materials **7**, 473 (2008).

[23] K. Garrity, A. Kakekhani, A. Kolpak, and S. Ismail-Beigi, Physical Review B **88**, 045401 (2013).

[24] A. M. Kolpak, I. Grinberg, and A. M. Rappe, Physical Review Letters **98**, 166101 (2007).

[25] Y. Inoue, I. Yoshioka, and K. Sato, Journal of Physical Chemistry **88**, 1148 (1984).

[26] Y. Yun, N. Pilet, U. D. Schwarz, and E. I. Altman, Surface Science **603**, 3145 (2009).

[27] M. P. McDaniel, Advances in Catalysis **33**, 47 (1985).

[28] D. Sanfilippo, F. Buonomo, G. Fusco, M. Lupieri, and I. Miracca, Chemical Engineering Science **47**, 2313 (1992).

[29] J. Baek, H. J. Yun, D. Yun, Y. Choi, and J. Yi, ACS Catalysis **2**, 1893 (2012).

[30] F. Ma, S. Chen, Y. Li, H. Zhou, A. Xu, and W. Lu, Applied Surface Science **313**, 654 (2014).

[31] D. Coulson, P. Wijnen, J. Lerou, and L. Manzer, Journal of Catalysis **140**, 103 (1993).

[32] S. C. York, and D. F. Cox, The Journal of Physical Chemistry B **107**, 5182 (2003).

[33] O. Dulub, U. Diebold, and G. Kresse, Physical Review Letters **90**, 016102 (2003).

[34] M. Kunat, S. G. Girol, T. Becker, U. Burghaus, and C. Wöll, Physical Review B **66**, 081402 (2002).

[35] B. Meyer, Physical Review B **69**, 045416 (2004).

[36] C. Wöll, Progress in Surface Science **82**, 55 (2007).

[37] J. V. Lauritsen *et al.*, ACS nano **5**, 5987 (2011).

[38] R. Wahl, J. V. Lauritsen, F. Besenbacher, and G. Kresse, Physical Review B **87**, 085313 (2013).

[39] H. Meskine, and P. A. Mulheran, Physical Review B **84**, 165430 (2011).

[40] J. S. Park *et al.*, Applied Surface Science **254**, 7786 (2008).

[41] J. S. Park *et al.*, Journal of Crystal Growth **311**, 2163 (2009).

[42] W. Gao, C. M. Wang, H. Q. Wang, V. E. Henrich, and E. I. Altman, Surface Science **559**, 201 (2004).

[43] M. W. Herdiech, X. Zhu, M. D. Morales-Acosta, F. J. Walker, and E. Altman, Physical Chemistry Chemical Physics **17**, 9488 (2015).

[44] T. M. Børseth, B. G. Svensson, and A. Y. Kuznetsov, Physica Scripta **126**, 10 (2006).

[45] J. V. Lauritsen *et al.*, ACS Nano **5**, 5987 (2011).

[46] X. Q. Wei, B. Y. Man, M. Liu, C. S. Xue, H. Z. Zhuang, and C. Yang, Physica B: Condensed Matter **388**, 145 (2007).

[47] S. Evans, Surface and interface analysis **18**, 323 (1992).

[48] P. J. Cumpson, Journal of Electron Spectroscopy and Related Phenomena **73**, 25 (1995).

[49] A. C. Neal Fairley, *The Casa Cookbook - Part 1: Recipes for XPS data processing* (Acolyte Science, 2005).

[50] M. P. Seah, and W. A. Dench, Surface and Interface Analysis **1**, 2 (1979).

[51] I. Spolveri, A. Atrei, B. Cortigiani, U. Bardi, A. Santucci, and D. Ghisletti, Surface Science **412**, 631 (1998).

[52] M. Galeotti, M. Torrini, U. Bardi, A. Santucci, and D. Ghisletti, Surface Science **375**, 63 (1997).

[53] R. W. Grimes, D. J. Binks, and A. B. Lidiard, Philosophical Magazine A **72**, 651 (1995).

[54] G. P. Halada, and C. R. Clayton, Journal of the Electrochemical Society **138**, 2921 (1991).

[55] I. Ikemoto, K. Ishii, S. Kinoshita, H. Kuroda, M. A. Franco, and J. Thomas, Journal of Solid State Chemistry **17**, 425 (1976).

[56] H. A. Bullen, and S. J. Garrett, Chemistry of Materials **14**, 243 (2002).

[57] J. Moulder, W. Stickle, P. Sobol, and K. Bomben, *Handbook of X-ray Photoelectron Spectroscopy* (Perkin-Elmer, Eden Prairie, MN, 1992).

[58] L. Piper, A. Preston, A. Fedorov, S. Cho, A. DeMasi, and K. Smith, Physical Review B **81**, 233305 (2010).

[59] G. Deroubaix, and P. Marcus, Surface and Interface Analysis **18**, 39 (1992).

[60] C. Sleigh, A. Pijpers, A. Jaspers, B. Coussens, and R. J. Meier, Journal of Electron Spectroscopy and Related Phenomena **77**, 41 (1996).

[61] A. Maetaki, and K. Kishi, Surface Science **411**, 35 (1998).

[62] D. C. Gleason-Rohrer, B. S. Brunschwig, and N. S. Lewis, The Journal of Physical Chemistry C **117**, 18031 (2013).

[63] E. I. Solomon, and V. Henrich, Surface Science Spectra **5**, 186 (1998).

[64] K. Ozawa *et al.*, Physical Review B **79**, 075314 (2009).

[65] W. Xiao, K. Xie, Q. Guo, and E. Wang, Journal of Physics: Condensed Matter **15**, 1155 (2003).

[66] X. Li, L. Liu, and V. E. Henrich, Solid State Communications **84**, 1103 (1992).

[67] S. Brunet, B. Requieme, E. Colnay, J. Barrault, and M. Blanchard, Applied Catalysis B: Environmental **5**, 305 (1995).

[68] D. Bechadergue, M. Blanchard, and P. Canesson, Applied Catalysis **20**, 179 (1986).

[69] J. Barrault, S. Brunet, B. Requieme, and M. Blanchard, J. Chem. Soc.-Chem. Commun. **4**, 374 (1993).

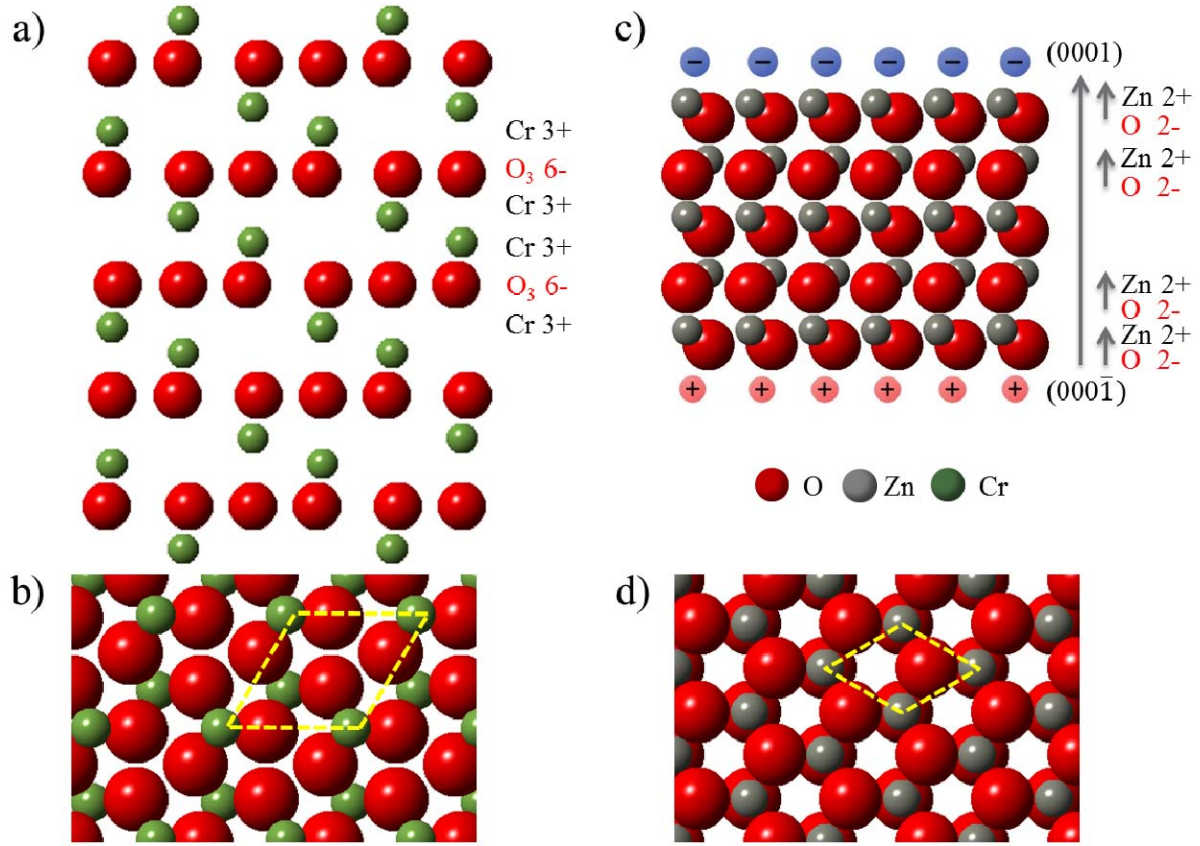[70] M. W. Mensch, C. M. Byrd, and D. F. Cox, Catalysis Today **85**, 279 (2003).

Figure 1. (Color online) a) Cross-sectional and b) top-down views of bulk-terminated Cr_2O_3 (0001). The Cr^{3+}-O^{6-}-Cr^{3+} repeat unit in b) lacks a dipole. c) Cross-sectional and d) top-down views of bulk-terminated ZnO   .   The small arrows in c) highlight the dipole due to the alternating Zn and O planes while the large arrow indicates the thickness-dependent dipole that would emerge in the absence of the compensating charges shown as pink and blue circles at the bottom and top of the illustration. In b) and d) the dotted lines highlight the surface unit cells. The models in b) and d) are drawn to the same scale to highlight the larger O atom spacing on the ZnO surface. The red balls represent O, the gray Zn, and the green Cr.
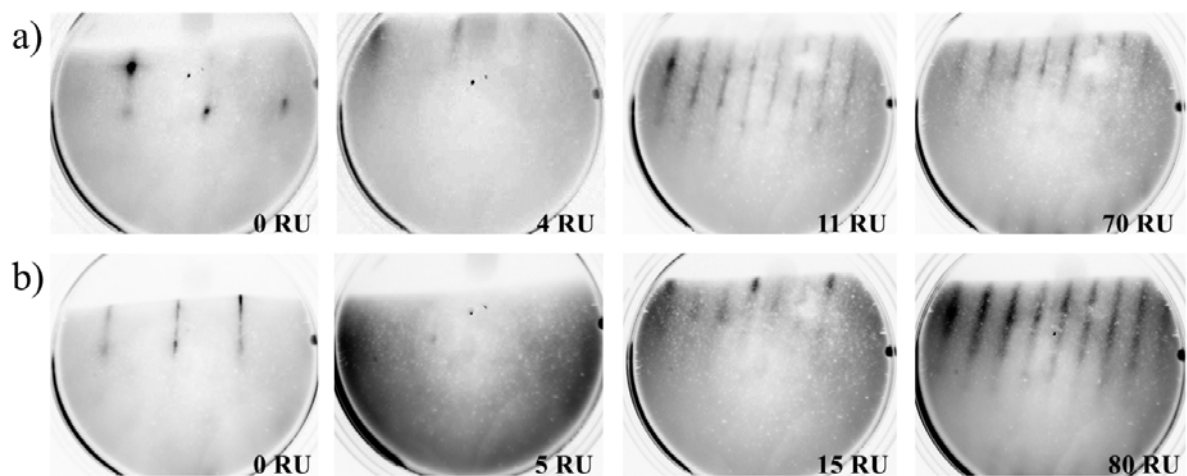
Figure 2. Evolution of RHEED patterns collected along the substrate [direction during Cr oxide growth at 845 K on a) ZnO   and b) ZnO   . The electron energy was 16 keV.
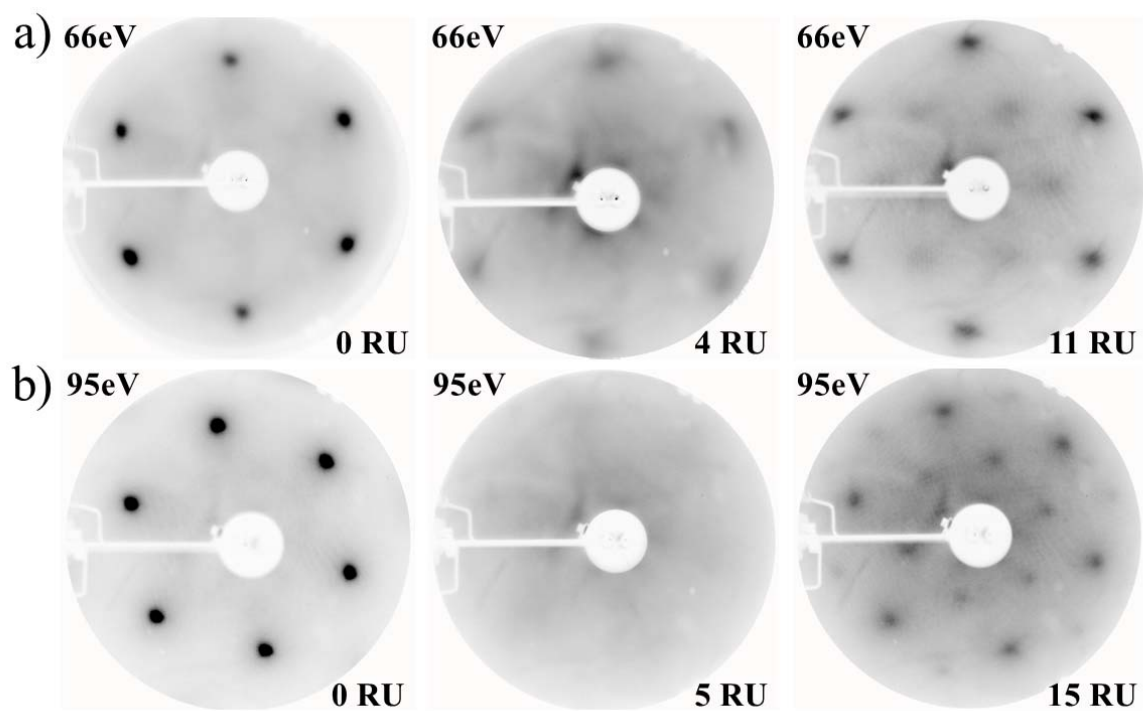
Figure 3. Series of LEED patterns showing the fading of the ZnO substrate LEED pattern and

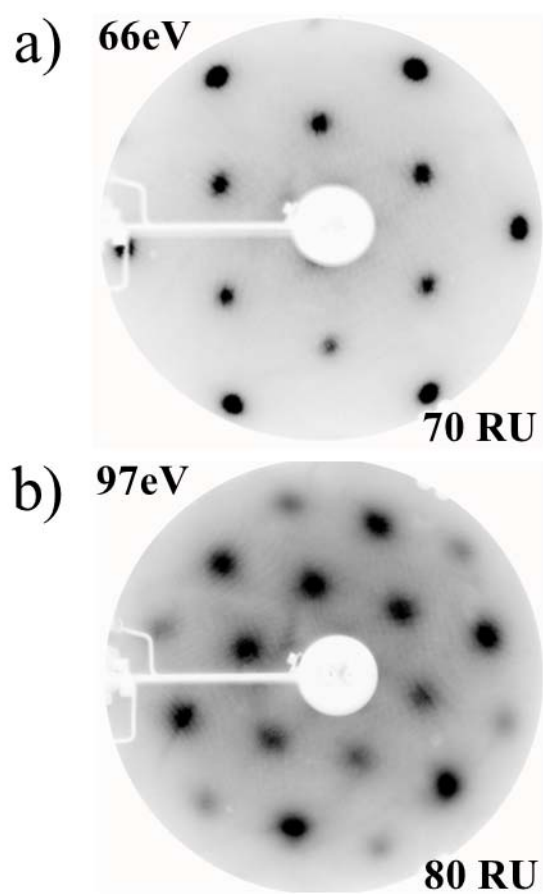the emergence of a new roughly ‾ ‾ pattern as Cr oxide is deposited onto a) ZnO

and b) ZnO .

28

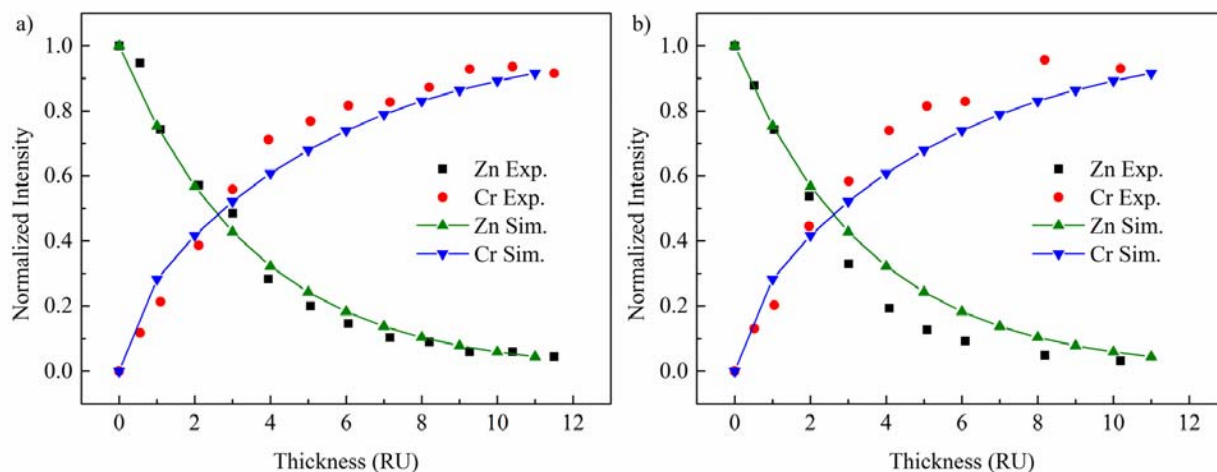**Figure 4.** LEED patterns for thick, bulk-like Cr_2O_3 grown on a) ZnO and b) ZnO

.

Figure 5. (Color online) Plots of the Zn 2p and Cr 2p XPS peak integrals normalized to the O 1s

peak integral as a function of Cr oxide thickness in equivalent RU of Cr_2O_3 for a) ZnO

and b) ZnO   . The thickness of a Cr_2O_3 repeat unit is taken as the 0.225 nm distance

between hexagonal oxygen planes along [0001]. The solid lines highlight the expected decay of

the Zn 2p and growth of the Cr 2p peaks assuming a 1.495 increase in O atom density across the

ZnO/Cr_2O_3 interface and electron mean free paths of 0.8 nm for Zn 2p and 1.21 nm for Cr 2p and

O 1s.
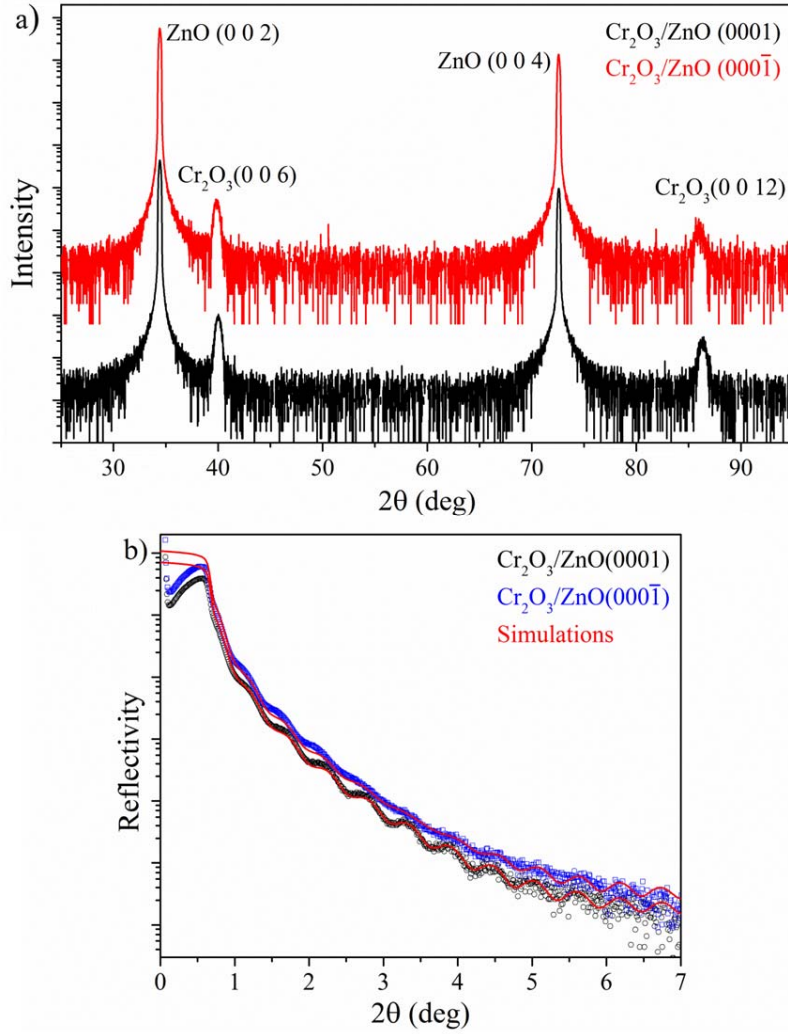
Figure 6. (Color online) a) X-ray diffraction θ−2θ scans for 15 nm (≈ 70 RU) Cr oxide on ZnO and 17 nm (≈ 80 RU) Cr oxide on ZnO with intensity presented on a logarithmic scale. The labels identify Zn and Cr oxide Bragg reflections that closely match the observed peak positions. The curves have been offset for clarity. b) Expanded view of the XRR profiles for the same films in a). The red lines highlight simulations with parameters (film thickness, density, surface and interface roughnesses) that best fit the data.
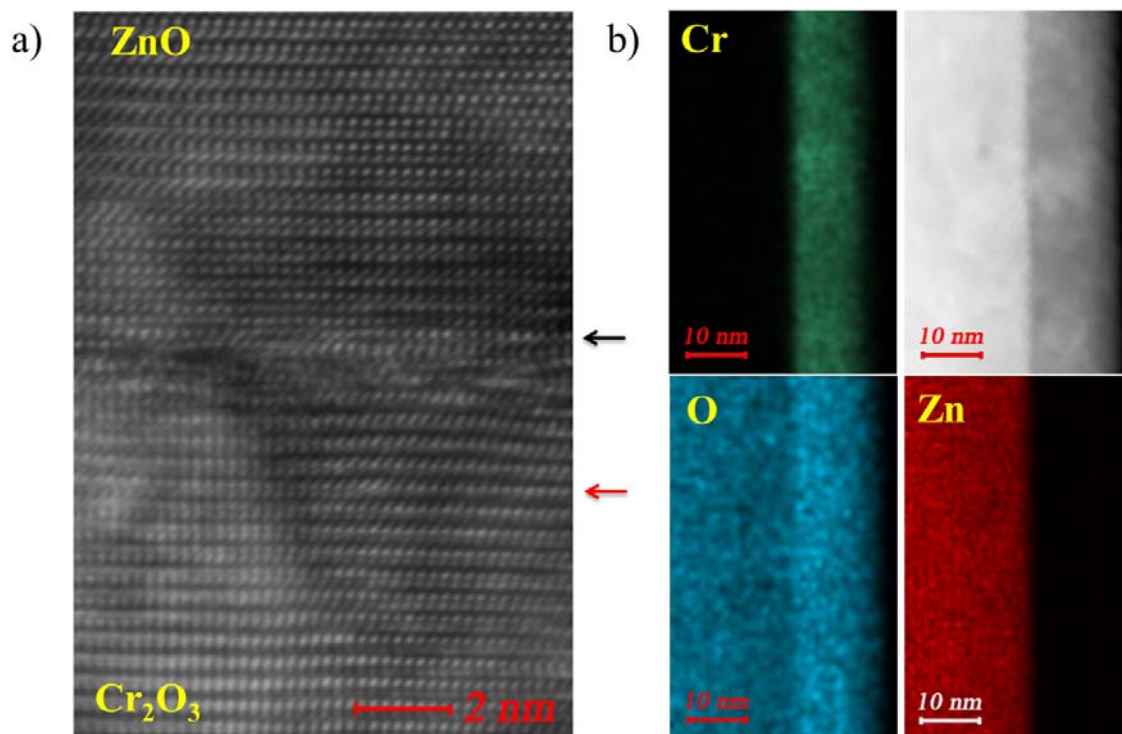
Figure 7. (Color online) a) High resolution cross-sectional electron micrograph of a 20 nm thick ($\approx$ 90 RU) Cr oxide film grown on ZnO with ZnO at the top and Cr_2O_3 at the bottom. The black arrow at the left points to the ZnO layer and the red arrow to the point in the Cr oxide film where surface electron diffraction suggests order begins to re-emerge. b) EDX maps for Cr, O and Zn recorded while obtaining the STEM image in the upper right; lighter shading indicates stronger emission for the elements indicated in the images. These data are for the same film in (a) and reveal an abrupt transition from Zn to Cr oxide.
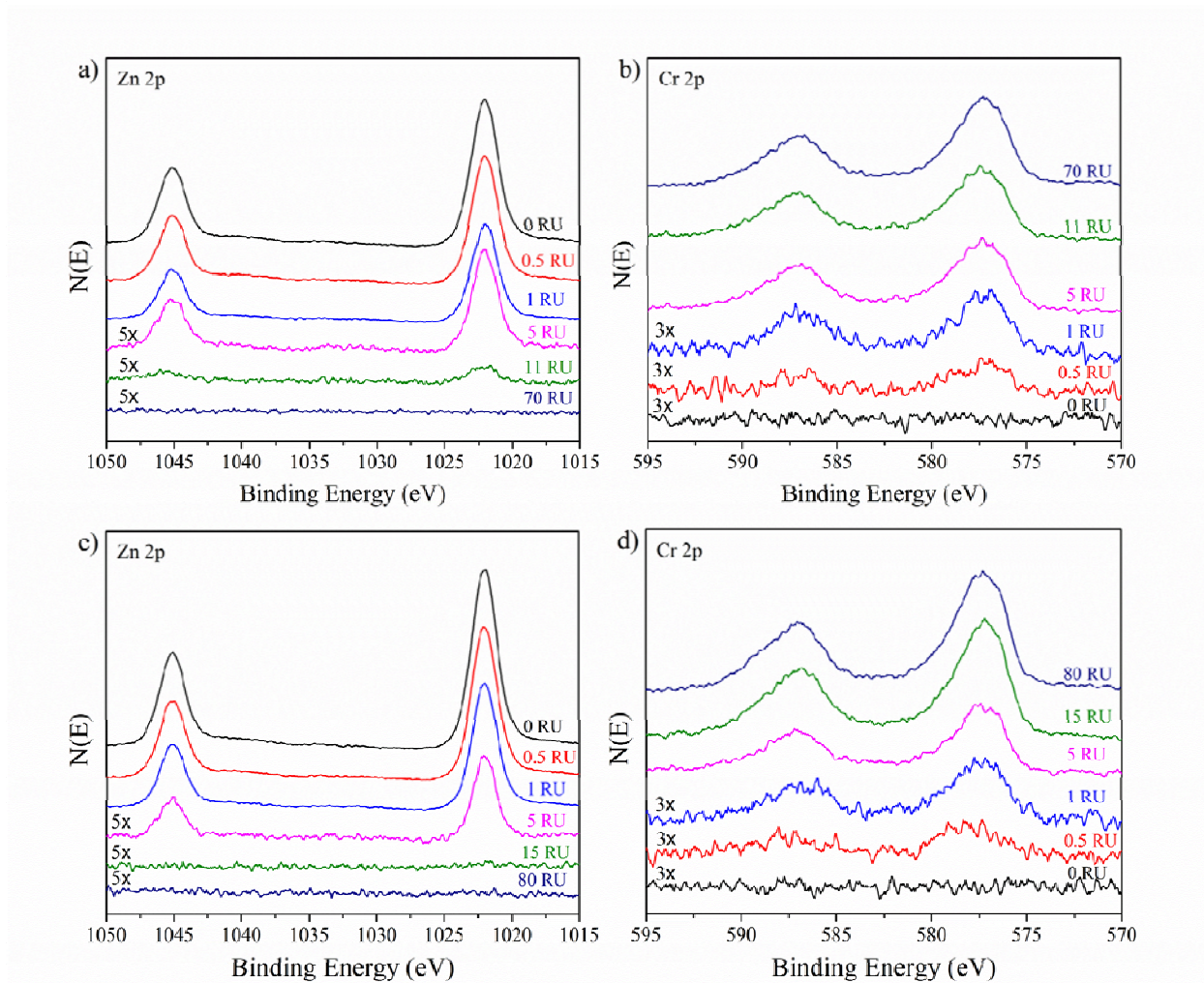
Figure 8. (Color online) Core level XPS spectra showing the evolution of the Zn 2p and Cr 2p regions as Cr oxide was added to a, b) ZnO   and c, d) ZnO   . Note that for films 15 RU and thicker, the Zn peak is completely attenuated and so instead the O 1s peak is used as the reference.

Figure 9. (Color online) Plot comparing the Cr $2p_{3/2}$ binding energy as a function of Cr oxide thickness for Cr oxide on ZnO (0001) (black squares) ZnO $(000\bar{1})$ (red circles). The binding energies are determined by fitting the spectra to mixed Gaussian-Lorentzian curves and the error bars from the uncertainties of these fits and the determination of the position of the reference Zn $2p_{3/2}$ peak.
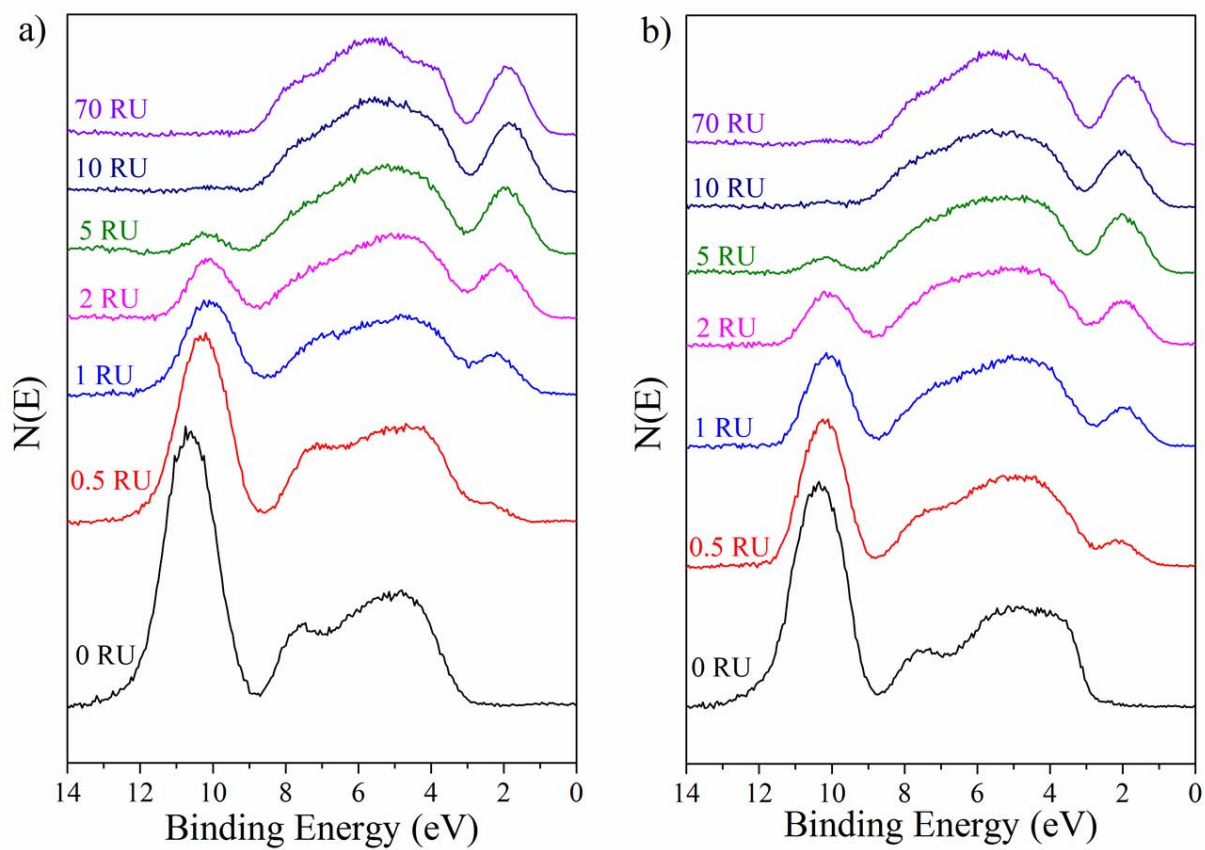
Figure 10. (Color online) Series of UPS spectra illustrating how the valence band changes with Cr oxide thickness on a) ZnO and b) ZnO . The spectra were collected with He II radiation at 40.8 eV, corrected for satellite lines and a Shirley background subtracted
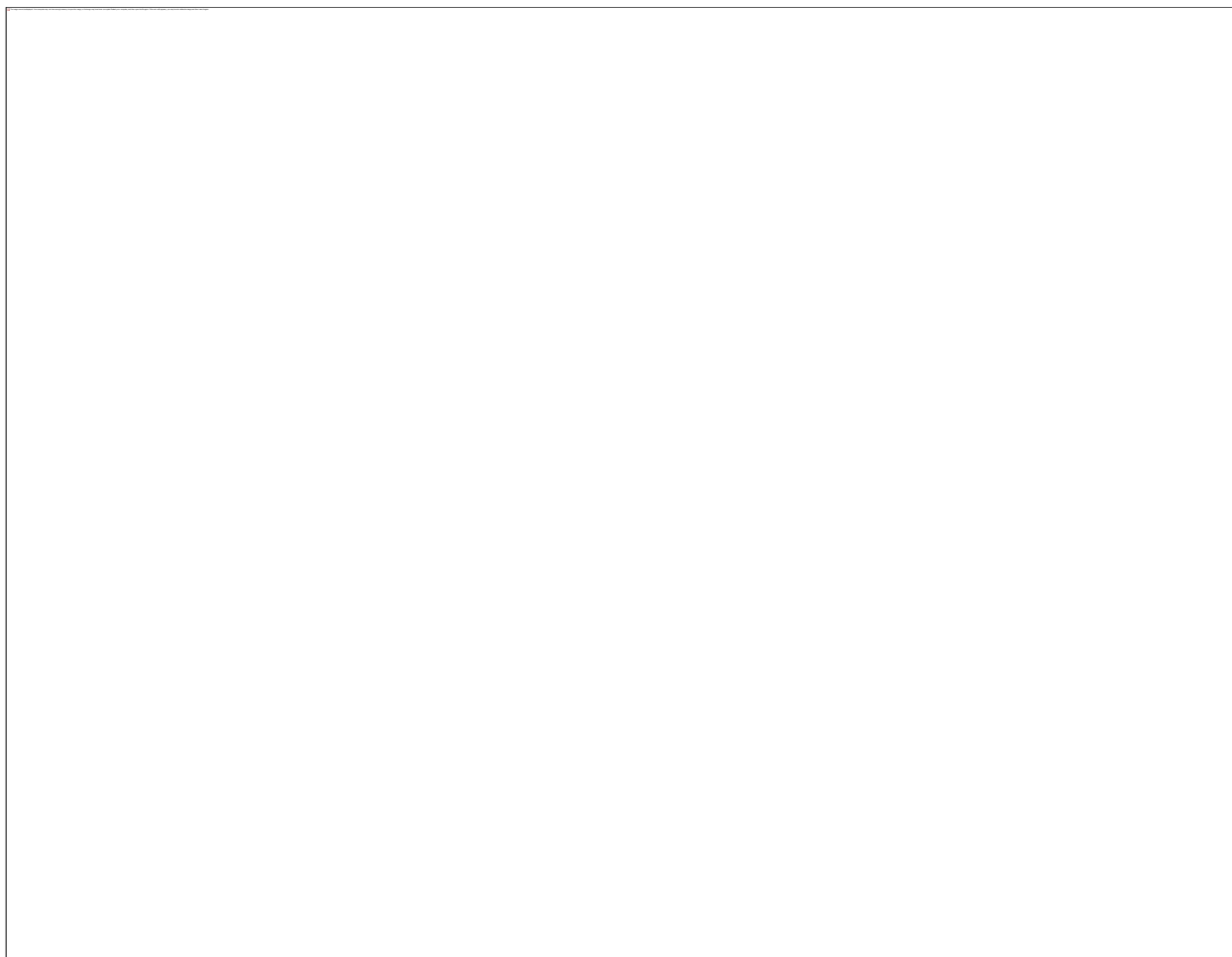
Figure 11. (Color online) Deconvolution of the UPS spectrum of 1 RU Cr_2O_3/ZnO (0001) into bulk ZnO (magenta) and Cr_2O_3 (green) components. The best fit of the experimental spectrum as a linear combination of bulk ZnO and Cr_2O_3 spectra is provided by the dotted red line. The blue line shows the residual between the experimental data and the best fit which can be associated with interface states and differences between repeat unit and bulk Cr_2O_3.
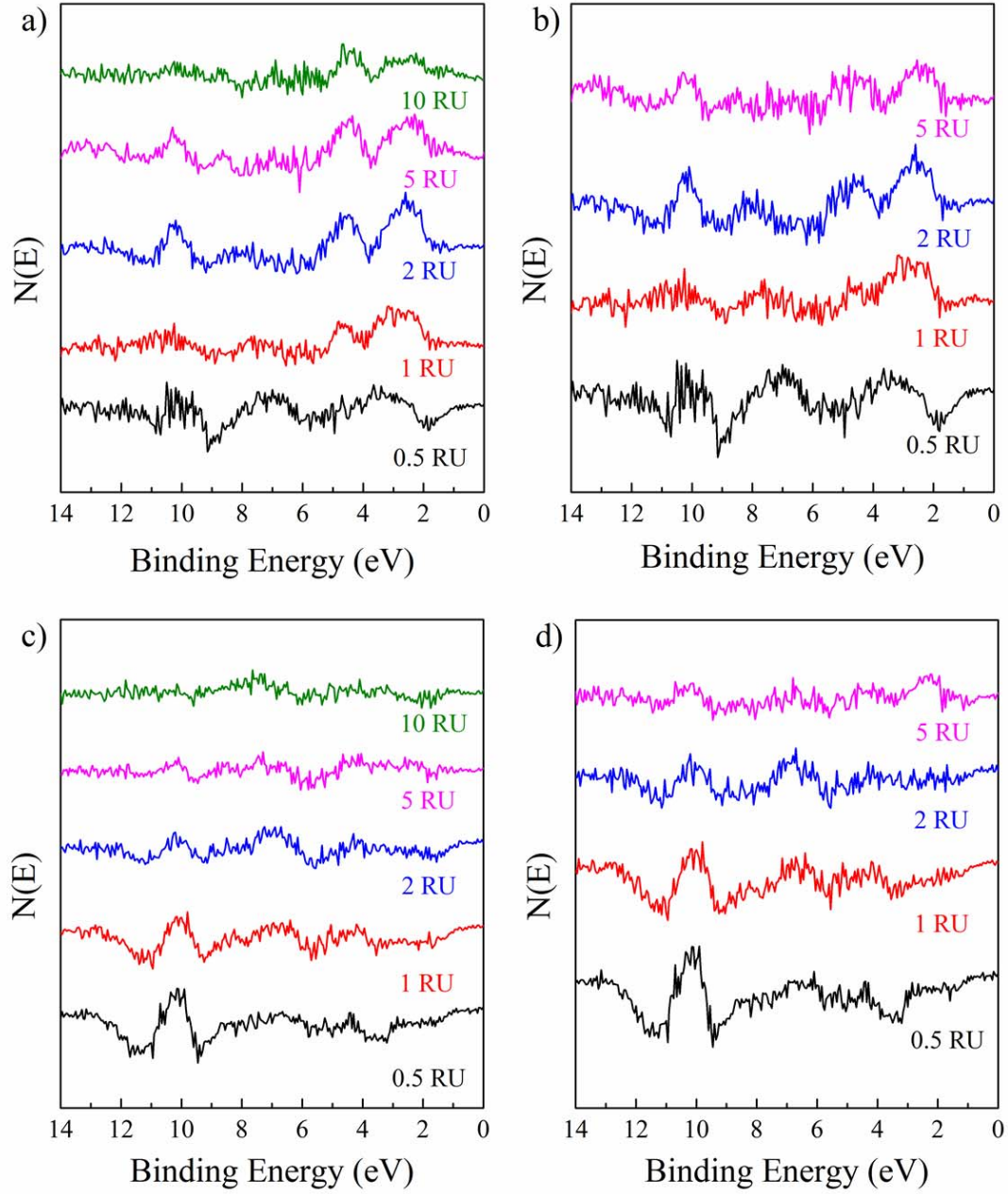
Figure 12. (Color online) Residual plots obtained after fitting UPS spectra for Cr_2O_3/ZnO as linear combinations of a) bare ZnO and 70 RU thick bulk-like Cr_2O_3 (0001) film spectra and b) bare ZnO and 10 RU Cr_2O_3/ ZnO spectra. c, d) same as a, b) except with ZnO as the substrate.